First Steps: Micro-CT Investigation of Frost Formation Using Stable Substitutes

A. Labuschagne,

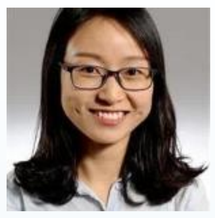

Dr. T. Zhu

Authors: Labuschagne A.[1], Zhu T. [1], Rohlfs W. [1]

[1]Department of Thermal and Fluid Engineering, University of Twente, Enschede, Netherlands

Prof.Dr.-Ing. W. Rohlfs

Background:

Air-source heat pumps promise significant energy usage and emissions reduction, but frost remains a significant concern. Frost formation on evaporator plates may reduce operating efficiency by up to 60 % [1]. Yet, effective frost mitigation strategies require an understanding of the frost formation dynamics and properties such as conductivity and diffusivity. Researchers have found it difficult to measure the fragile frost structures without significant interference and thus the process of formation is not fully understood, especially regarding internal crystal structure [2]. In this study, we attempt to use Micro-CT scanning to observe these structurally dependent properties of frost.

Materials and methods:

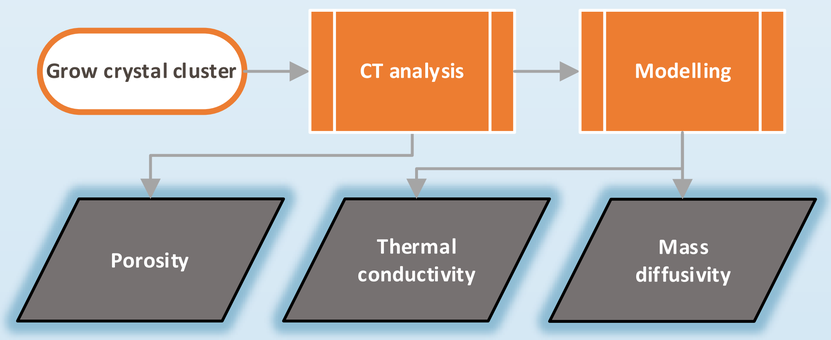

As an initial step towards measuring frost accurately and in situ, urea was proposed as a first substitute for evaluating the methodological feasibility.

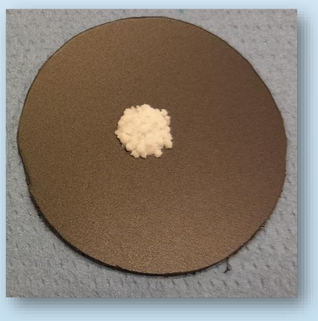

After scanning the urea sample, noise was removed using the Daubechies 1 wavelet filter. The resulting image was segmented, and floating islands were removed before cropping. To calculate the local properties of the sample, the 3D steady-state diffusion equation was solved:

$$0 = \frac{\partial\left(\mathrm{D}\frac{\partial\Phi}{\partial \mathrm{x}}\right)}{\partial \mathrm{x}} + \frac{\partial\left(\mathrm{D}\frac{\partial\Phi}{\partial \mathrm{y}}\right)}{\partial \mathrm{y}} + \frac{\partial\left(\mathrm{D}\frac{\partial\Phi}{\partial \mathrm{z}}\right)}{\partial \mathrm{z}}$$

using the boundary conditions:

- Top – (273 K, 80 % RH)
- Bottom – (263K, 100 % RH)
- Sides – Symmetric boundary conditions

The resulting matrix was used in conjunction with two methods for calculating the local diffusivity and conductivity:

A. A simple averaging of the properties in each z-layer.
B. A calculation of the (per layer) properties by utilizing the ideal series and ideal parallel resistance models as per:

$$\gamma_{\text{parallel}} = \gamma_{\text{ice}} \cdot \varphi + \gamma_{\text{air}} \cdot (1-\varphi),$$

$$\gamma_{\text{series}} = \left(\frac{\varphi}{\gamma_{\text{ice}}} + \frac{(1-\varphi)}{\gamma_{\text{air}}}\right)^{-1}$$

Results:

The figure below shows the temperature profile along the sample (PP-base) surface as a colour gradient. The crystal structure was found to be needle-like with two structural zones in the lower and upper ends respectively, each with their unique thermophysical properties.

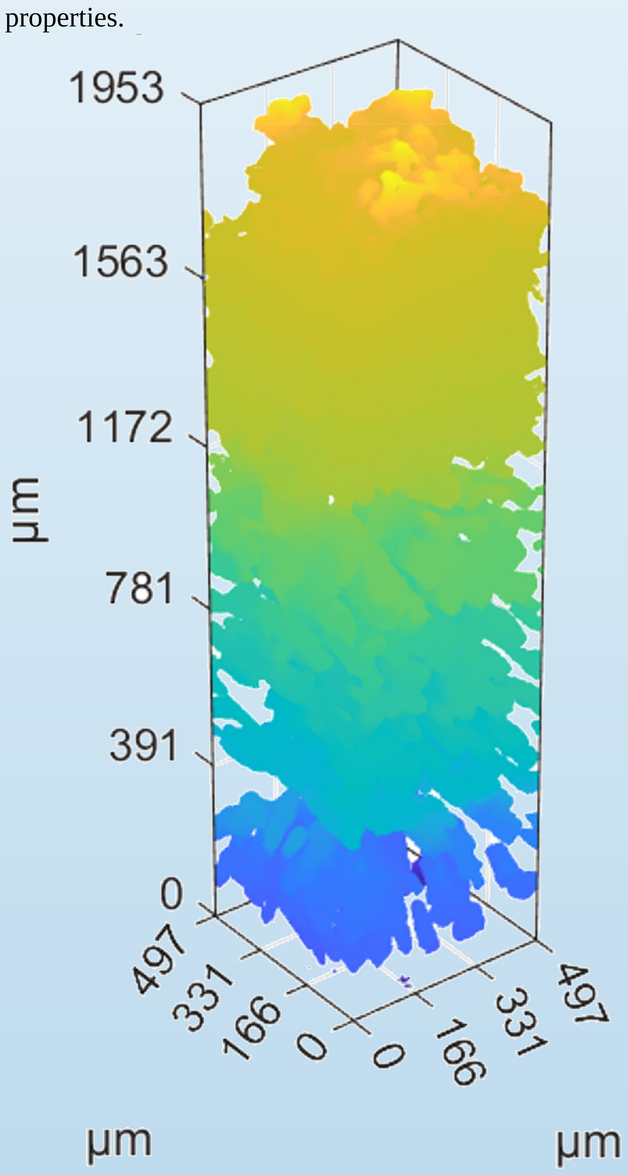

The effective thermal conductivity was found to be 0.136 W/m.K, with an overall density as 387 kg/m3 and effective mass diffusivity of 3.92 mm2/s.

The following figures compare the effective thermal conductivity determined by method A, represented by the solid, orange line, to that of method B, represented by the dotted, orange lines as well as showing the general correlations to the sample density, the solid, blue line.

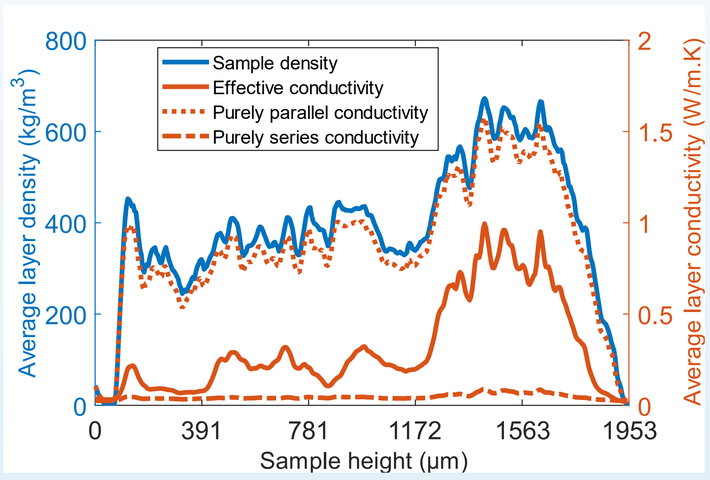

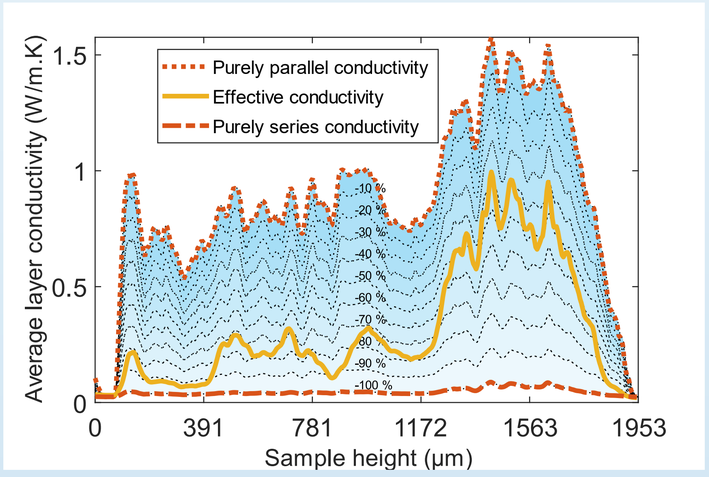

Method A produces a realistic view of the local sample properties by accounting for the interconnected nature of the crystal layers. Method B produces an idealized picture of the sample properties. In the next figure, we see that the calculated effective thermal conductivity does not take some weighted average value between the two ideals, as some models assume, but varies according to the specific crystal structures in the local, and neighbouring layers.

Conclusion:

The successful scanning, segmentation and evaluation of the urea sample confirms the proposed methodological feasibility. Structural effects have been observed to cause deviation from standard bulk-weighted models and new observations regarding the structural contributions to thermophysical properties should be made.

Next steps:

1. Construction of frost environmental chamber
2. In-situ frost growth and scanning
3. Frost growth modelling

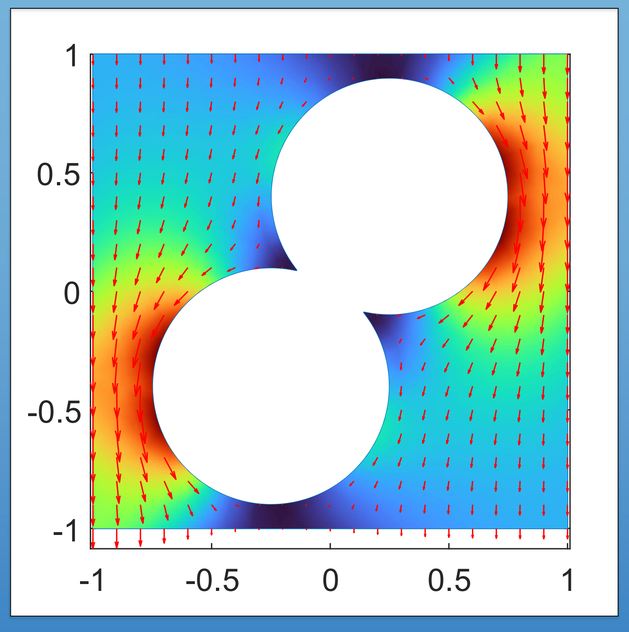

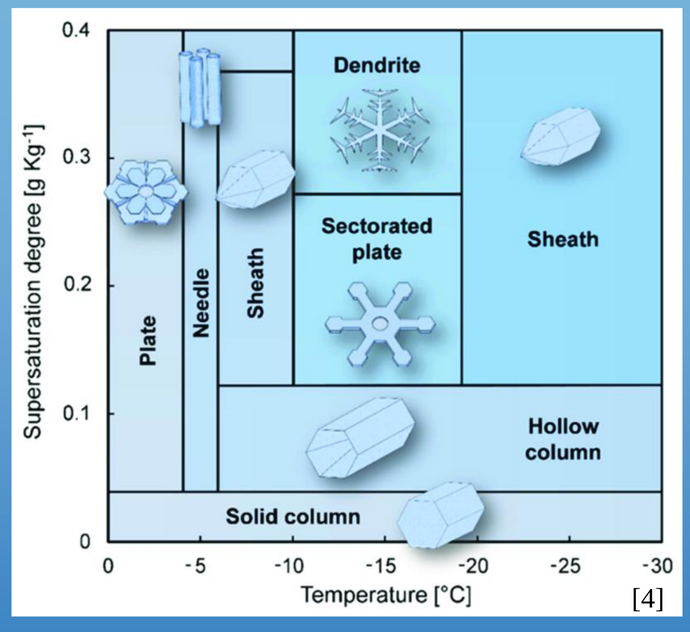

[4]

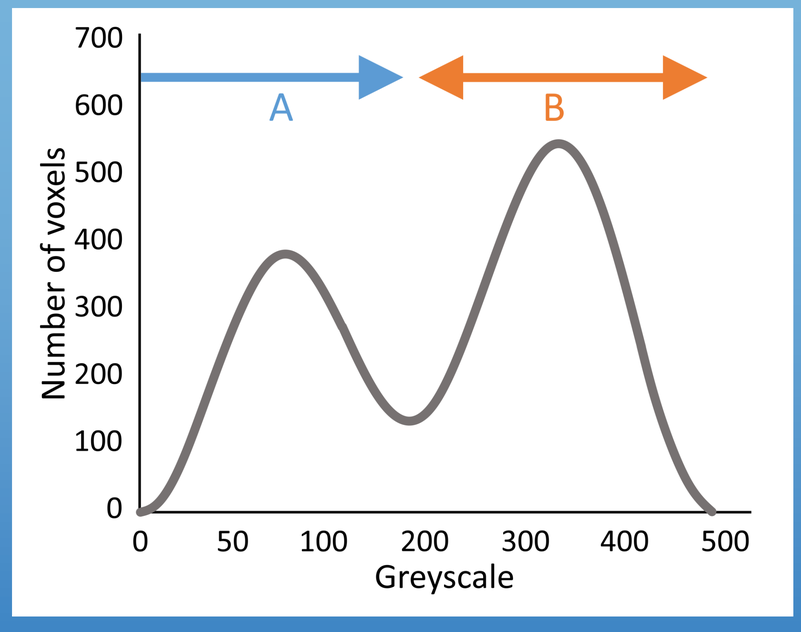

References:

[1] Y. Li, M. Li, Y. Utaka, T. Daitoku, H. Ohkubo, and C. Yang, *Int. J. Refrig.*, 101, pp. 148–154, (2019).

[2] A. Leoni, M. Mondot, F. Durier, R. Revellin, and P. Haberschill, *Exp. Therm. Fluid Sci.*, 88, pp. 220–233, (2017).

[3] Object Research Systems (ORS) Inc, Retrieved Dec. 15, 2022, from https://theobjects.com/dragonfly/index.html, (2022).

[4] C. J. L. Hermes, J. Boeng, D. L. da Silva, F. T. Knabben, and A. D. Sommers, "Evaporator Frosting in Refrigerating Appliances: Fundamentals and Applications," Energies (Basel), vol. 14, no. 18, p. 5991, 2021.

UNIVERSITY OF TWENTE.